Transmit Adaptivity for Cognitive Radar

Antonio De Maio
Università degli Studi di Napoli "Federico II"
Dipartimento di Ingegneria Elettrica e delle Tecnologie dell'Informazione
Via Claudio 21, I-80125 Napoli, Italy
ademaio@unina.it

Alfonso Farina
Technical Consultant
previous with Selex ES (now retired) Rome, Italy
alfonso.farina@outlook.it

ABSTRACT

Radar signal design in a spectrally crowded environment is a very challenging and topical problem due to the increasing demand of both military surveillance/remote sensing capabilities and civilian wireless services. This work deals with the synthesis of optimized radar waveforms ensuring spectral compatibility with the overlayed licensed electromagnetic radiators. Cognition provided by a Radio Environmental Map (REM) is exploited as the key to an intelligent dynamic spectrum allocation. In fact, the information provided by the REM is exploited to force dynamic spectral constraints on the radar waveform which is thus the result of a constrained optimization process aimed at improving some radar performances (such as detection, sidelobes, resolution, tracking). A solution technique leading to an optimal waveform is proposed. The procedure requires the relaxation of the original problem into a convex optimization problem and involves a polynomial computational complexity.

1. Introduction

Coexistence among radar and telecommunication systems is a crucial issue which has been attracting the interest of many scientists and engineers during the last few years and is currently becoming one of the challenging research topics in both radar and communication communities [1]. The even growing demand of both high quality wireless services and accurate remote sensing capabilities is, in fact, increasing the amount of required bandwidth [2], [3]. Furthermore, basic electromagnetic considerations, such as good foliage penetration [4], and low path loss attenuation, push some communication and radar systems to coexist in the same frequency band [5] (for instance VHF and UHF). As a result, the electromagnetic spectrum is becoming more and more crowded. It is thus imperative the development of advanced radar signals ensuring compatibility with the surrounding electromagnetic radiators, namely keeping acceptable the mutual interference induced on frequency overlayed systems.

Many papers in open literature have considered the problem of designing radar waveforms with a suitable frequency allocation [6], so as to control the interference brought on overlayed wireless networks (communication and navigation systems), while enhancing radar performance requirements in terms of range-Doppler resolution, low range and Doppler sidelobes, detection and tracking capabilities. In [7], a waveform design technique is introduced to confer some desired spectral nulls to the radar signal. The idea is to perturb a stepped frequency modulated pulse forcing an additional fast time polyphase code. An alternate projection algorithm for the construction of chirp-like constant-modulus signals with a single spectral null is proposed in [8], whereas in [9] its extension, addressing the production of multiple notches, is established. Some iterative algorithms are introduced in [10] for the joint design of the transmit signal and the receive filter achieving frequency stop-band suppression and range sidelobes minimization. A genetic algorithm to design sparse waveforms for high frequency surface wave radar systems is investigated in [11]. In [12], a fast coding technique based on alternate projections and successive fast Fourier transforms is developed to obtain sparse waveforms with a controlled Peak Sidelobe Level (PSL). In [13] and [14], sparse frequency constant modulus radar signals with a low Integrated Sidelobe Level (ISL) are built optimizing a suitable combination between the ISL metric and a penalty function accounting for the waveform frequency allocation. Finally, in [15], a spectrum-centric signal design is developed based on the minimization of the transmitted energy on a set of disjoint stop-band frequencies under a unimodularity constraint and AutoCorrelation Function (ACF) masking.

Herein, a cognitive procedure [16]–[18] is proposed to devise radar waveforms sharing desirable spectral features which ensure coexistence with overlayed wireless networks, and optimizing radar detection performance. It is supposed that the radar system has the ability to predict the behavior of surrounding licensed radiators, for instance using a Radio Environmental Map (REM), [19], containing geographical features, available wireless services and their spectral regulations, locations and activities of wireless transmitters. This is the key to a cognitive adaptation since the aforementioned information enable an intelligent spectrum utilization in a spectrally crowded environment. More in details, the proposed design technique considers as figure of merit the Signal to Interference plus Noise Ratio (SINR) and optimizes the transmitted radar waveform constraining the amount of interference energy on crowded/reserved frequency bands. Other than an energy constraint, a similarity constraint is enforced on the transmitted radar signal, so as to control some relevant characteristics of the waveform, such as range-Doppler resolution, variations in the signal modulus, and PSL. The resulting problem can be formalized as a non-convex optimization Quadratically Constrained Quadratic Programming (QCQP) problem. It is worth pointing out that the similarity and the spectral compatibility constraints are generally competing, namely it is not always ensured the existence of a radar code compliant with both of them. This motivates a

study of the Interference/Similarity (I/S) achievable region, namely the set of the admissible interference and similarity levels. Remarkably, it is shown the convexity of the aforementioned set, which leads to the achievability of all the I/S levels contained in the convex hull of any I/S feasible pairs. With reference to the solution technique adopted for the considered design problem, first of all it is relaxed into a convex one which belongs to the SemiDefinite Programming (SDP) problem class. Then an optimum waveform is constructed through a specific rank-one decomposition of [20] performed on an optimal solution to the relaxed convex problem. Remarkably the entire procedure entails a polynomial computational complexity. It is worth pointing out that, there is no algorithm available in the open literature, capable of optimizing the SINR, while constraining and controlling, at the same time, both the produced interference power as well as the shape of the transmitted waveform. Indeed, the available techniques only focus on the control of the interference power and the shape of the signal, without accounting for the achieved SINR. On the other hand, our algorithm can be used for improving, in the SINR sense, any waveform devised through any other algorithm, while keeping under control the interference produced by the waveform, as well as its shape.

2. System Model & Problem Formulation

Let $c(t)$ be the baseband equivalent of the transmitted radar pulse, assumed to be composed of N linearly modulated sub-pulses; the code element for the i-th sub-pulse is denoted $c(i)$ and the vector $\boldsymbol{c} = [c(1), \ldots, c(N)]^T \in \mathbb{C}^N$ represents the fast-time radar code. The waveform at the receiver end is down-converted to baseband, undergoes a sub-pulse matched filtering operation, and then is sampled.

The N-dimensional column vector $\boldsymbol{v} = [v(1), \ldots, v(N)]^T \in \mathbb{C}^N$ of the fast time observations, associated to the range-azimuth cell under test, can be expressed as:

$$\boldsymbol{v} = \alpha_T \boldsymbol{c} + \boldsymbol{n}, \tag{1}$$

with α_T a complex parameter accounting for channel propagation and backscattering effects from the target within the range-azimuth bin of interest, and $\boldsymbol{n}$ the N-dimensional column vector containing the filtered disturbance echo samples. Specifically, the vector $\boldsymbol{n}$ accounts for both white internal thermal noise and interfering signals due to unknown and unlicensed, possibly hostile jammers as well as licensed overlayed telecommunication networks sharing the same frequencies as the radar of interest. Moreover, $\boldsymbol{n}$ is modeled as a complex, zero-mean, circularly symmetric Gaussian random vector with covariance matrix $\mathbb{E}[\boldsymbol{n}\boldsymbol{n}^\dagger] = \boldsymbol{M}$.

As to the licensed radiators coexisting with the radar of interest, we suppose that each of them is working over a frequency band $\Omega_k = \left[f_1^k, f_2^k\right]$, $k = 1, \ldots, K$, where f_1^k and f_2^k denote the lower and upper normalized frequencies for the k-th system, respectively. To guarantee spectral compatibility with the overlayed telecommunication services, the radar has to control the amount of interfering energy produced on the shared frequency bands. From an analytical point of view, the amount of energy transmitted on the k-th band can be computed as

$$\int_{f_1^k}^{f_2^k} S_c(f)\, df \quad = \quad \boldsymbol{c}^\dagger \boldsymbol{R}_I^k \boldsymbol{c}, \tag{2}$$

where

$$S_c(f) = \left| \sum_{n=0}^{N-1} \boldsymbol{c}(n) e^{-j2\pi f n} \right|^2$$

is the Energy Spectral Density (ESD) of the fast-time code $\boldsymbol{c}$ and

$$\boldsymbol{R}_I^k(m,l) = \begin{cases} f_2^k - f_1^k & m = l \\ \dfrac{e^{j2\pi f_2^k(m-l)} - e^{j2\pi f_1^k(m-l)}}{j2\pi(m-l)} & m \neq l \end{cases} \qquad (m,l) \in \{1,\ldots,N\}^2. \tag{3}$$

For K radiators, the total interfering energy transmitted on the coexisting systems is given by

$$\sum_{k=1}^{K} \boldsymbol{c}^\dagger \boldsymbol{R}_I^k \boldsymbol{c}\,. \tag{4}$$

Hence, denoting by E_I the amount of allowed interference, to overlay the radar with coexisting telecommunication networks, the transmitted waveform has to comply with the constraint

$$\boldsymbol{c}^\dagger \boldsymbol{R}_I \boldsymbol{c} \leq E_I, \tag{5}$$

where

$$\boldsymbol{R}_I = \sum_{k=1}^{K} w_k \boldsymbol{R}_I^k. \tag{6}$$

It is worth pointing out that, by suitably choosing the coefficients $w_k \geq 0$, $k = 1,\ldots,K$, different weights can be given to the coexisting wireless networks, for instance based on their distance from the radar and their tactical importance (i.e. navigation systems, military communications, public services, etc).

A. Cognitive Spectrum Awareness

To quantify and control the amount of interference induced on coexisting telecommunication networks, radar requires the knowledge of the number K of coexisting licensed radiators, their bandwidth (referred to as stop-band in the following and defined by the lower and upper normalized frequencies f_1^k and f_2^k), and the penalty weights w_k's to assign to each competing system (see equation (6)). It is thus of paramount importance for the sensing radar to have an accurate, reliable, and comprehensive radio environment awareness. Radio Environment Map (REM) [19] represents the key to gain the aforementioned spectrum cognizance which is at the base of an intelligent and agile spectrum management. First introduced by the Virginia Tech team [22] as the main foundation for a novel approach to *Cognitive Radio* (CR) networking, REM can be considered as an *abstraction* of real-world radio scenarios, and can be considered as an integrated database digitizing and indexing the available electromagnetic information.

Figure 1 illustrates some REM multi-domain knowledge sources represented by geographical features, available services and spectral regulations, locations and activities of telecommunication networks, previous radio experiences and measurements [23]. Indeed, the idea behind REM is to store and process a variety of data, so as to make possible the inference of a multitude of environmental characteristics, such as locations of transmitters, prevailing propagation conditions, and estimates of spectrum usage over time and space. Thus, REM offers a suitable vehicle of CR system support, which can be exploited by cognitive engines for most cognitive functionalities, such as situation awareness, learning, reasoning, planning, and decision support.

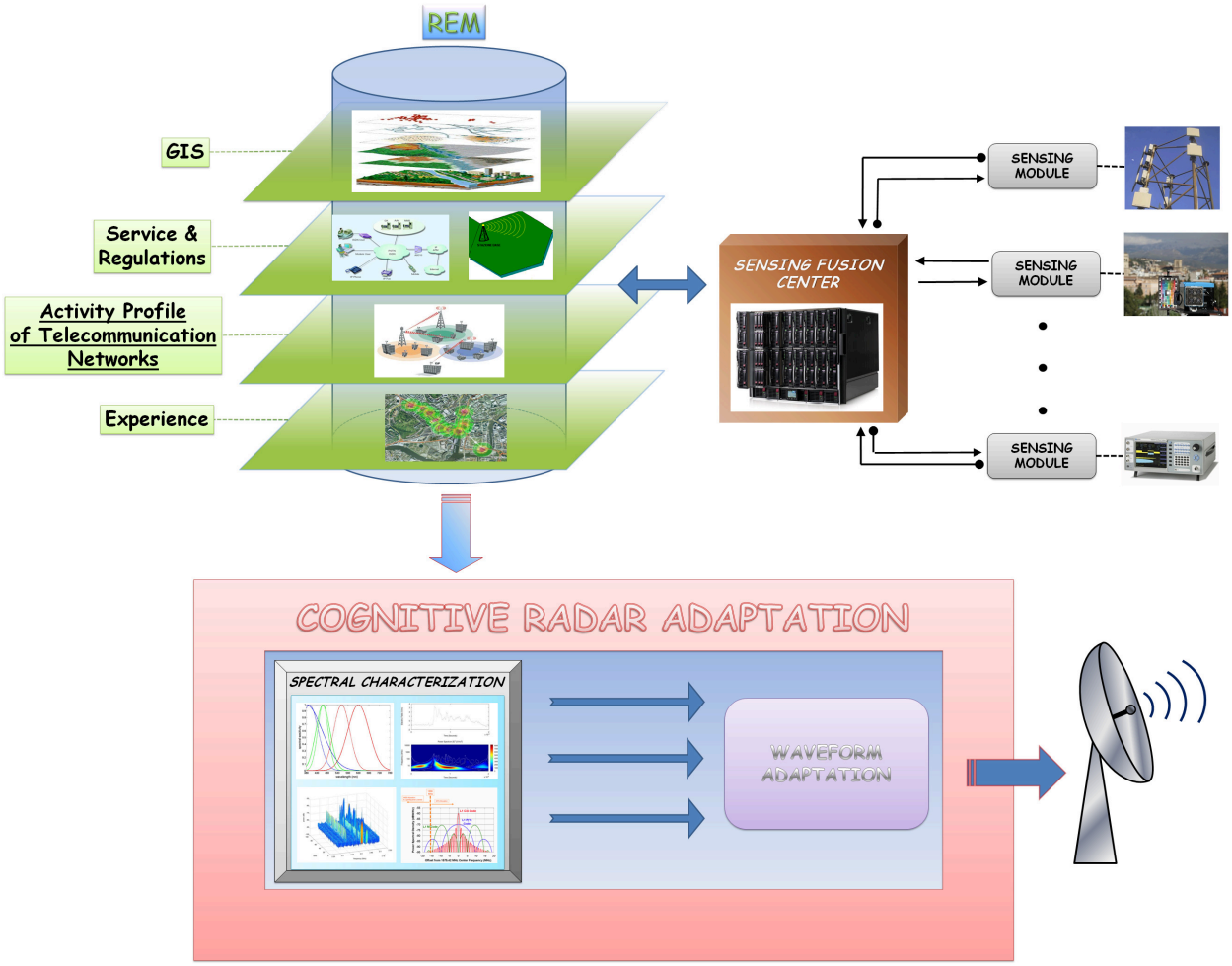

Figure 1: A pictorial representation of the REM and its usage in a cognitive radar.

To populate and update the REM, both a-priori knowledge as well as spectral sensing techniques (like feature-based signal detectors) can be used [23]. Furthermore, as depicted in the Figure 1, a dedicated sensor network could be also employed to improve the quality of the scenario monitoring. Obviously, the better the characterization and modeling of the radio environment, the more the system can benefit by a-priori information and past experiences and adapt to the operational environment. Therefore, the capability and the level of situation awareness may greatly impact the performance achieved by the CR system.

3. Code Design

In this section, we propose a waveform design technique which attempts to maximizing the detection probability and at the same time provides a control both on the interfering energy produced in the stop-

bands and on desirable features of the transmitted waveform. Precisely, we consider as figure of merit the SINR, defined as

$$\text{SINR} = |\alpha_T|^2 \boldsymbol{c}^\dagger \boldsymbol{R} \boldsymbol{c}\,, \tag{7}$$

where $\boldsymbol{R} = \boldsymbol{M}^{-1}$. Furthermore, to ensure coexistence among the radar and wireless telecommunication infrastructures sharing the same spectrum, we enforce the transmitted waveform to be compliant with the constraint (5). Finally, we impose an energy constraint $\boldsymbol{c}^\dagger \boldsymbol{c} = 1$ as well as a similarity constraint [24] between the sought radar code and a unit energy reference code $\boldsymbol{c}_0$ ($\|\boldsymbol{c}_0\|^2 = 1$)

$$\|\boldsymbol{c} - \boldsymbol{c}_0\|^2 \leq \epsilon\,, \tag{8}$$

where the parameter $\epsilon \geq 0$ rules the size of the similarity region. It is worth pointing out that designing a code which optimizes the detection performance does not provide any kind of control on the shape of the resulting coded waveform. Otherwise stated, an unconstrained optimization can lead to signals with significant modulus variations, poor range resolution, high PSLs, and more in general an undesired ambiguity function behavior. Forcing (8), when $\boldsymbol{c}_0$ shares constant modulus, reasonable range resolution and PSL, allows to indirectly control desirable features of the radar waveform. The smaller ϵ, the higher the degree of similarity between the designed radar code and $\boldsymbol{c}_0$.

Based on the aforementioned guidelines, the waveform design problem can be formulated as a non-convex QCQP optimization problem

$$\text{P}_1 \begin{cases} \max_{\boldsymbol{c}} & \boldsymbol{c}^\dagger \boldsymbol{R} \boldsymbol{c} \\ \text{s.t.} & \boldsymbol{c}^\dagger \boldsymbol{c} = 1 \\ & \boldsymbol{c}^\dagger \boldsymbol{R}_I \boldsymbol{c} \leq E_I \\ & \|\boldsymbol{c} - \boldsymbol{c}_0\|^2 \leq \epsilon \end{cases},$$

which can be equivalently written as

$$\text{P}_2 \begin{cases} \max_{\boldsymbol{c}} & \boldsymbol{c}^\dagger \boldsymbol{R} \boldsymbol{c} \\ \text{s.t.} & \boldsymbol{c}^\dagger \boldsymbol{c} = 1 \\ & \boldsymbol{c}^\dagger \boldsymbol{R}_I \boldsymbol{c} \leq E_I \\ & \text{Re}\left(\boldsymbol{c}^\dagger \boldsymbol{c}_0\right) \geq 1 - \epsilon/2 \end{cases}. \tag{9}$$

Notice that previously proposed code design procedures [7], [9], [13], [15], can be applied for the construction of a high quality reference code, namely a code exhibiting desired spectral properties as well as radar features. By doing so, moving in a suitable Euclidean ball centered in the aforementioned code we can improve the radar performance still keeping spectral coexistence.

The feasibility of problem P_1, which not only depends on the parameters E_I and ϵ but also on the pre-fixed code $\boldsymbol{c}_0$, is discussed in the next subsection, whereas the technique adopted to solve problem P_2 is presented in subsection **3-A**.

A. Solution to the Optimization Problem

In this subsection, we show how an optimal solution to the non-convex optimization problem P_2 can be computed in polynomial time. First of all, let us observe that an optimal solution to P_2 can be obtained from an optimal solution to the following Enlarged Quadratic Problem (EQP):

$$\text{P}_3 \begin{cases} \max_{\boldsymbol{c}} & \boldsymbol{c}^\dagger \boldsymbol{R} \boldsymbol{c} \\ \text{s.t.} & \boldsymbol{c}^\dagger \boldsymbol{c} = 1 \\ & \boldsymbol{c}^\dagger \boldsymbol{R}_I \boldsymbol{c} \leq E_I \\ & \text{Re}^2\left(\boldsymbol{c}^\dagger \boldsymbol{c}_0\right) + \text{Im}^2\left(\boldsymbol{c}^\dagger \boldsymbol{c}_0\right) = \boldsymbol{c}^\dagger \boldsymbol{c}_0 \boldsymbol{c}_0{}^\dagger \boldsymbol{c} \geq \delta_\epsilon \end{cases} \tag{10}$$

where $\delta_\epsilon = (1-\epsilon/2)^2$. In fact, since the feasible region of P_3 is larger than that of P_2, every optimal solution of P_3, which is feasible for P_2, is also an optimal solution for P_2 [25]. Thus, assume that $\bar{\boldsymbol{c}}$ is an optimal solution to P_3 and let $\phi = \arg(\bar{\boldsymbol{c}}^\dagger \boldsymbol{c}_0)$. It is easily seen that $\bar{\boldsymbol{c}}e^{j\phi}$ is still an optimal solution to P_3. Now, observing that $(\bar{\boldsymbol{c}}e^{j\phi})^\dagger \boldsymbol{c}_0 = |\bar{\boldsymbol{c}}^\dagger \boldsymbol{c}_0|$, $\bar{\boldsymbol{c}}e^{j\phi}$ is a feasible solution to P_2. In other words, $\bar{\boldsymbol{c}}e^{j\arg(\bar{\boldsymbol{c}}^\dagger \boldsymbol{c}_0)}$ is optimal for both P_2 and P_3.

Now, we have to find an optimal solution to P_3 and, to this end, we exploit the equivalent matrix formulation

$$\mathrm{P}_3 \begin{cases} \max_{\boldsymbol{C}} & \mathrm{tr}(\boldsymbol{C}\boldsymbol{R}) \\ \text{s.t.} & \mathrm{tr}(\boldsymbol{C}) = 1 \\ & \mathrm{tr}(\boldsymbol{C}\boldsymbol{R}_I) \le E_I \\ & \mathrm{tr}(\boldsymbol{C}\boldsymbol{C}_0) \ge \delta_\epsilon \\ & \boldsymbol{C} = \boldsymbol{c}\boldsymbol{c}^\dagger \end{cases} \tag{11}$$

where $\boldsymbol{C}_0 = \boldsymbol{c}_0 \boldsymbol{c}_0{}^\dagger$. All the non-convexity of problem P_3 is now confined in the rank-one constraint $\boldsymbol{C} = \boldsymbol{c}\boldsymbol{c}^\dagger$.

Problem (11) can be relaxed into a convex SDP optimization problem, neglecting the rank-one constraint [26]. By doing so, we obtain an Enlarged Quadratic Problem Relaxed (EQPR)

$$\mathrm{P}_4 \begin{cases} \max_{\boldsymbol{C}} & \mathrm{tr}(\boldsymbol{C}\boldsymbol{R}) \\ \text{s.t.} & \mathrm{tr}(\boldsymbol{C}) = 1 \\ & \mathrm{tr}(\boldsymbol{C}\boldsymbol{R}_I) \le E_I \\ & \mathrm{tr}(\boldsymbol{C}\boldsymbol{C}_0) \ge \delta_\epsilon \\ & \boldsymbol{C} \succeq \boldsymbol{0} \end{cases} . \tag{12}$$

Let us now observe that problem P_4 is solvable; in fact, the feasible constraints set is a compact set (closed and bounded) and the objective function of P_4 is continuous; furthermore, assuming that problem P_1 is strictly feasible, problem P_4 is strictly feasible. This property can be of paramount importance from a numerical point of view, since it guarantees that at any optimal point the complementary conditions are satisfied [27] and interior point methods [25] can be used.

In order to prove the hidden convexity of problem P_3, namely that the relaxation of P_3 into P_4 is tight, we construct a rank-one optimal solution $\bar{\boldsymbol{c}}\bar{\boldsymbol{c}}^\dagger$ to P_4, starting from an arbitrary rank optimal solution $\bar{\boldsymbol{C}}$ to problem P_4. To this end, we resort to the rank-one matrix decomposition theorem [20, Theorem 2.3], which is cited as the following lemma [1].

Lemma 3.1: Let $\boldsymbol{X}$ be a non-zero $N \times N$ ($N \ge 3$) complex Hermitian positive semidefinite matrix and $\{\boldsymbol{A}_1, \boldsymbol{A}_2, \boldsymbol{A}_3, \boldsymbol{A}_4\}$ be Hermitian matrices, and suppose that $(\mathrm{tr}(\boldsymbol{Y}\boldsymbol{A}_1), \mathrm{tr}(\boldsymbol{Y}\boldsymbol{A}_2), \mathrm{tr}(\boldsymbol{Y}\boldsymbol{A}_3), \mathrm{tr}(\boldsymbol{Y}\boldsymbol{A}_4)) \ne (0,0,0,0)$ for any non-zero complex Hermitian positive semidefinite matrix $\boldsymbol{Y}$ of size $N \times N$. Then,

- if $\mathrm{rank}(\boldsymbol{X}) \ge 3$, one can find, in polynomial time, a rank-one matrix $\boldsymbol{x}\boldsymbol{x}^\dagger$ such that $\boldsymbol{x}$ (synthetically denoted as $\boldsymbol{x} = \mathcal{D}_1(\boldsymbol{X}, \boldsymbol{A}_1, \boldsymbol{A}_2, \boldsymbol{A}_3, \boldsymbol{A}_4)$) is in $\mathrm{range}(\boldsymbol{X})$, and

$$\boldsymbol{x}^\dagger \boldsymbol{A}_i \boldsymbol{x} = \mathrm{tr}(\boldsymbol{X}\boldsymbol{A}_i), \quad i = 1,2,3,4;$$

[1] Function $\mathcal{D}_1$ and $\mathcal{D}_2$ are useful to schematize the mapping (formally defined and proved in [20, Theorem 2.3]) between an arbitrary rank matrix $\boldsymbol{X}$ and a rank one matrix $\boldsymbol{x}\boldsymbol{x}^\dagger$, satisfying $\mathrm{tr}(\boldsymbol{X}\boldsymbol{A}_i) = \mathrm{tr}(\boldsymbol{x}\boldsymbol{x}^\dagger \boldsymbol{A}_i)$, $i = 1,2,3,4$. As to the MATLAB codes implementing the functions $\mathcal{D}_1$ and $\mathcal{D}_2$, please see http://www.math.hkbu.edu.hk/~huang/index-2.htm.

- if rank $(\boldsymbol{X}) = 2$, for any $\boldsymbol{z}$ not in the range space of $\boldsymbol{X}$, one can find a rank-one matrix $\boldsymbol{x}\boldsymbol{x}^\dagger$ such that $\boldsymbol{x}$ (synthetically denoted as $\boldsymbol{x} = \mathcal{D}_2(\boldsymbol{X}, \boldsymbol{A}_1, \boldsymbol{A}_2, \boldsymbol{A}_3, \boldsymbol{A}_4)$) is in the linear subspace spanned by $\{\boldsymbol{z}\} \cup$ range $(\boldsymbol{X})$, and
$$\boldsymbol{x}^\dagger \boldsymbol{A}_i \boldsymbol{x} = \text{tr}\,(\boldsymbol{X}\boldsymbol{A}_i), \quad i = 1, 2, 3, 4.$$

Let us check the applicability of Lemma 3.1 to both $\bar{\boldsymbol{C}}$ and the matrix parameters of P_4. Indeed, the condition $N \geq 3$ is mild and practical (the number of transmitted pulses is usually greater than or equal to 3). Now, in order to verify

$$(\text{tr}\,(\boldsymbol{Y}\boldsymbol{R}), \text{tr}\,(\boldsymbol{Y}\boldsymbol{I}), \text{tr}\,(\boldsymbol{Y}\boldsymbol{R}_I), \text{tr}\,(\boldsymbol{Y}\boldsymbol{C}_0)) \neq (0, 0, 0, 0), \text{ for any non-zero } \boldsymbol{Y} \succeq 0,$$

it suffices to prove that there is $(a_1, a_2, a_3, a_4) \in \mathbb{R}^4$ such that

$$a_1\boldsymbol{R} + a_2\boldsymbol{I} + a_3\boldsymbol{R}_I + a_4\boldsymbol{C}_0 \succ \boldsymbol{0}.$$

But this is evident for the matrix parameters of P_4. As a consequence, after constructing a rank-one optimal solution $\bar{\boldsymbol{c}}\bar{\boldsymbol{c}}^\dagger$ to P_4, an optimal solution to P_1 is given by $\boldsymbol{c}^\star = \bar{\boldsymbol{c}} e^{j \arg(\bar{\boldsymbol{c}}^\dagger \boldsymbol{c}_0)}$. **Algorithm 1** summarizes the procedure leading to an optimal solution to P_1.

Algorithm 1 : Algorithm for Cognitive Radar Code Optimization

Input: $\boldsymbol{c}_0$, $\boldsymbol{R}$, $\boldsymbol{R}_I$, E_I, δ_ϵ.
Output: An optimal solution $\boldsymbol{c}^\star$ to P_1.
1: solve SDP P_4 finding an optimal solution $\bar{\boldsymbol{C}}$ and the optimal value $v^\star$;
2: **if** rank $(\bar{\boldsymbol{C}}) = 1$ **then**
3: set $\bar{\boldsymbol{c}} = \lambda_{\max}(\bar{\boldsymbol{C}})\boldsymbol{v}$, with $\boldsymbol{v}$ being an eigenvector associated to the maximum eigenvalue of $\bar{\boldsymbol{C}}$;
4: **else if** rank $(\bar{\boldsymbol{C}}) = 2$ **then**
5: find $\bar{\boldsymbol{c}} = \mathcal{D}_2\left(\bar{\boldsymbol{C}}, \boldsymbol{R}, \boldsymbol{I}, \boldsymbol{R}_I, \boldsymbol{C}_0\right)$;
6: **else**
7: find $\bar{\boldsymbol{c}} = \mathcal{D}_1\left(\bar{\boldsymbol{C}}, \boldsymbol{R}, \boldsymbol{I}, \boldsymbol{R}_I, \boldsymbol{C}_0\right)$;
8: **end**
9: output $\boldsymbol{c}^\star = \bar{\boldsymbol{c}} e^{j \arg(\bar{\boldsymbol{c}}^\dagger \boldsymbol{c}_0)}$.

The computational complexity connected with the implementation of the algorithm is polynomial as both the SDP problem and the decomposition of Lemma 3.1 can be performed in polynomial time.

4. Performance Analysis

In this section, we assess the performance of the proposed waveform design technique in terms of achievable SINR value, spectral shape, and autocorrelation features. Specifically, we study the I/S achievable region of problem P_1 for a fixed interfering scenario, and analyze the behavior of the waveforms devised according to **Algorithm 1**.

We consider a radar whose baseband equivalent transmitted signal has a two-sided bandwidth of 810 kHz and it is sampled at $f_s = 810$ kHz. As to the interference, we suppose that it is composed of unlicensed narrowband continuous jammers, white interference, and licensed coexisting telecommunication

networks spectrally overlayed to the radar of interest. Specifically, we model the disturbance covariance matrix as:

$$\boldsymbol{M} = \sigma_0 \boldsymbol{I} + \sum_{k=1}^{K} \frac{\sigma_{I,k}}{\Delta f_k} \boldsymbol{R}_I^k + \sum_{k=1}^{K_J} \sigma_{J,k} \boldsymbol{R}_{J,k}, \tag{13}$$

where

- $\sigma_0 = 0$ dB is the thermal noise level;
- $K = 7$ is the number of licensed radiators;
- $\sigma_{I,k}$ accounts for the energy of the k-th coexisting telecommunication network operating on the normalized frequency band $[f_2^k, f_1^k]$ ($\sigma_{I,k} = 10$ dB, $k = 1, \ldots, K$);
- $\Delta f_k = f_2^k - f_1^k$ is the bandwidth associated with the k-th licensed radiator, for $k = 1, \ldots, K$;
- $K_J = 2$ is the number of active and unlicensed narrowband jammers;
- $\sigma_{J,k}$, $k = 1, \ldots, K_J$, accounts for the energy of the k-th active jammer ($\sigma_{J,1\,\text{dB}} = 50$ dB, $\sigma_{J,2\,\text{dB}} = 40$ dB);
- $\boldsymbol{R}_{J,k}$, $k = 1, \ldots, K_J$, is the normalized disturbance covariance matrix of the k-th active unlicensed jammer, defined as

  $$\boldsymbol{R}_{J,k} = \boldsymbol{r}_{J,k} \boldsymbol{r}_{J,k}^{\dagger},$$

  with $r_{J,k}(n) = e^{j2\pi f_{J,k} n / f_s}$, where $f_{J,k}$ denotes the Doppler shift of the k-th jammer ($f_{J,1}/f_s = 0.7$, and $f_{J,2}/f_s = 0.75$).

As to the overlayed and foreseen telecommunication systems, which spectrally coexist with the radar of interest, we consider the following baseband equivalent radar stop-bands [28]:

$$\begin{array}{lll} \Omega_1 = [0.0000, 0.0617]\,, & \Omega_2 = [0.0988, 0.2469]\,, & \Omega_3 = [0.2593, 0.2840]\,, \\ \Omega_4 = [0.3086, 0.3827]\,, & \Omega_5 = [0.4074, 0.4938]\,, & \Omega_6 = [0.5185, 0.5556]\,, \\ \Omega_7 = [0.9383, 1.0000]\,. & & \end{array} \tag{14}$$

Furthermore, we suppose licensed/foreseen overlayed systems with the same relevance, namely $w_k = 1$ for $k = 1, \ldots, 7$. Based on the assumed stop-bands (14) and weights w_k's, we can compute the matrix $\boldsymbol{R}_I$, defined in (6), and enforce the interference energy constraint on the transmitted radar waveform. Notice that, the matrix $\boldsymbol{R}_I$ does not depend on the frequencies of the unlicensed jammers and is only function of the spectral bands (14) and weights associated to the licensed radiators.

As to the reference waveform $\boldsymbol{c}_0$, we model it as a unitary norm Linear Frequency Modulated (LFM) pulse with a duration of 200 μsec and a chirp rate $K_s = (750 \times 10^3)/(200 \times 10^{-6})$ Hz/sec; it results in $N = 162$ samples due to the considered sampling frequency.

Finally, for comparison purpose, with reference to the example of Figures 3, we consider the transmit sequence $\tilde{\boldsymbol{c}}_0$ and the receive filter $\tilde{\boldsymbol{g}}_0$ devised through the procedure in [10]. Specifically, with reference to the *soft-power constraint* transmit waveform design technique [10], we assume, as starting sequence, the code $\boldsymbol{c}_0$, and fix $\delta = 0.9$, $\lambda_T = 10^{-5}$, and $\boldsymbol{R}^{(2)} = \boldsymbol{R}_I$, whereas, with reference to the receive filter design technique, we fix $\beta = 0.05$, $\lambda_T = 10^{-5}$, $\Delta n = 10$, and assume $\boldsymbol{R}^{(2)} = \boldsymbol{M}$ (more details about the Lindenfeld's algorithms, the aforementioned parameters, and their setting, can be found in [10]).

The I/S achievable region for the considered scenario is represented in Figure 2. Notice that the radar designer can choose the pair (E_I, ϵ), referred to in the sequel as operative point, to suitably trade off spectral coexistence, desirable radar waveform characteristics and achievable SINR of the system. For instance, with reference to Figure 2, considering (E_I, ϵ) equal to the point A, the frequency coexistence of the radar with the overlayed telecommunication networks is emphasized, with respect to choosing (E_I, ϵ) equal to the point B. In the last case, other radar features, such as high range-Doppler resolution and/or low sidelobe levels, are privileged.

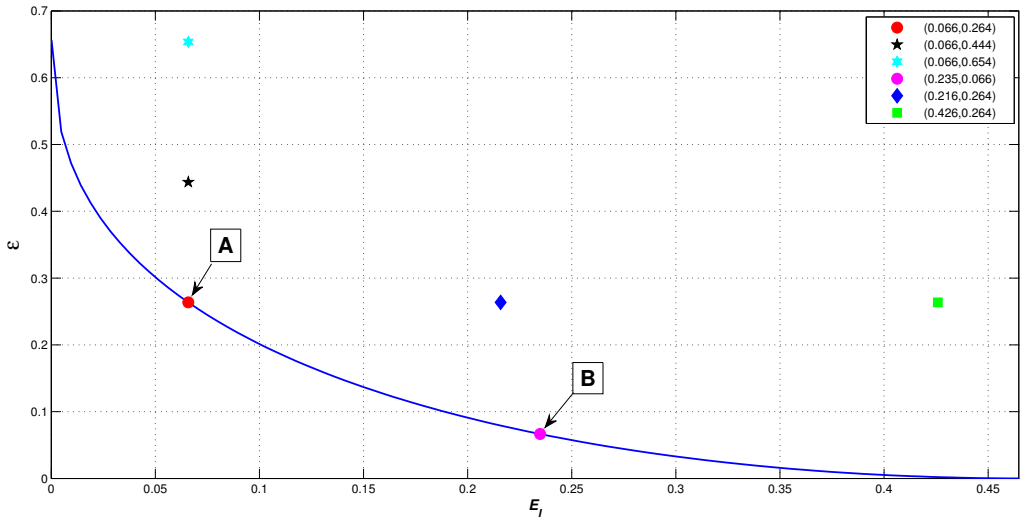

Figure 2: I/S achievable region, for chirp similarity code with an interference environment modeled as $K = 7$ equivalent stop-bands.

A. Behavior of the Devised Waveforms

In Figures 3, we provide the ESD, the squared modulus of the ACF, and the normalized SINR of the waveforms devised for three operative points (red dot, black star, and cyan hexagram in Figure 2). Specifically, we consider the points $(\hat{E}_I, \epsilon_n)$, $n = 1, 2, 3$, with $\hat{E}_I = 0.066$, $\epsilon_1 = 0.264$, $\epsilon_1 = 0.444$, $\epsilon_1 = 0.654$ (notice that $(\hat{E}_I, \epsilon_1)$ corresponds to the point **A** in Figure 2), and compare the results with those achievable by the couple signal/receiver $(\tilde{\boldsymbol{c}}_0, \tilde{\boldsymbol{g}}_0)$. In Figure 3(a), we plot the ESD of the synthesized signals versus the normalized frequency, together with that of the reference code. The stop-bands correspond to the ON-level of the red line, while the OFF-levels denote the frequencies where no foreseen system is transmitting. The curves highlight the capability of the proposed technique to suitably control the amount of energy produced over the shared frequency bands. In fact, for each ϵ, the energy transmitted in the stop-bands is lower than the allowed level, thus ensuring the coexistence with other transmitting systems.

However, we observe that, given the considered setting for the design parameters, the transmit signal $\tilde{\boldsymbol{c}}_0$ is capable of ensuring an even greater suppression of the interference at the stop-bands than the devised codes $\boldsymbol{c}$. Nevertheless, this behavior is quite expected as the signal design technique of [10] only focuses on the coexistence problem. In other words, the figure of merit is represented by the interference reduction, and no additional constraints are forced neither on the shape of the sought waveform (whose auto-ambiguity properties are unpredictable) nor on the SINR at the receiver side. On the contrary, the aim of the proposed algorithm is to maximize the attainable SINR, offering at the same time a control over the total amount of interference produced at certain frequencies, as well as on the resulting signal shape.

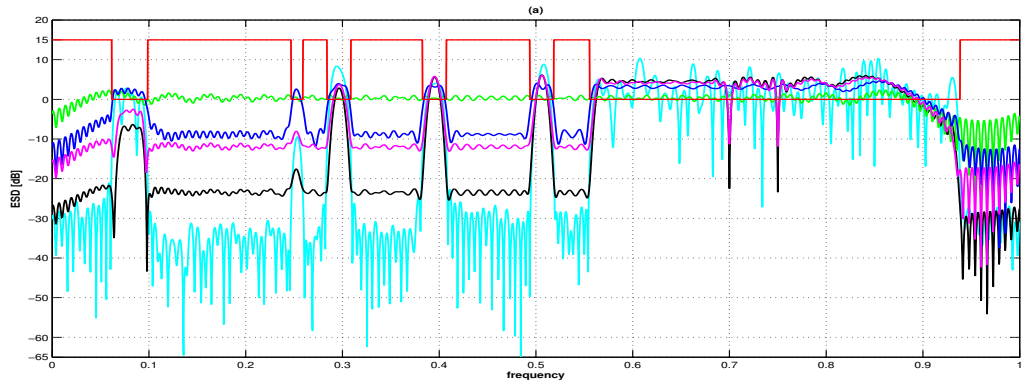

(a)

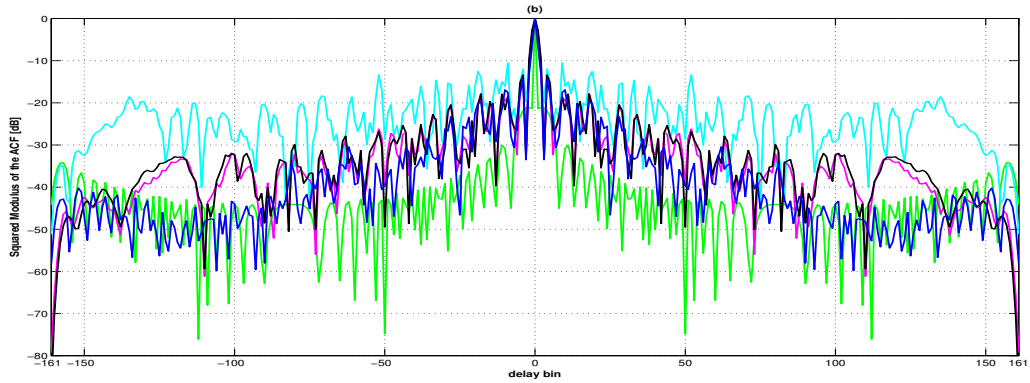

(b)

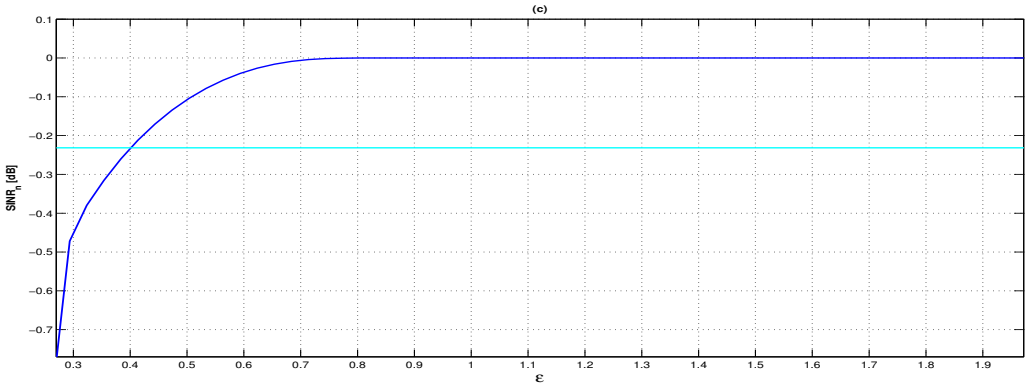

Figure 3: a) ESD; b) Squared modulus of the ACF. red dash-dotted lines: stop-bands; green curve: reference code $\boldsymbol{c}_0$; blue curve: **Algorithm 1**, $E_I = 0.066$, $\epsilon = 0.264$; magenta curve: **Algorithm 1**, $E_I = 0.066$, $\epsilon = 0.444$; black curve: **Algorithm 1**, $E_I = 0.066$, $\epsilon = 0.654$; cyan curve: Algorithm [10] c) blue curve: **Algorithm 1**, Normalized SINR vs ϵ, $E_I = 0.066$; cyan curve: $\tilde{\boldsymbol{c}}_0$, Algorithm [10].

Additionally, we notice that increasing the similarity parameter ϵ, namely increasing the available degrees of freedom, smarter and smarter distributions of the useful energy are achieved. Otherwise stated, **Algorithm 1** allows the designer to exactly choose the amount of energy suppression to force over the stop-bands, which is instead not possible with reference to the procedure of [10]. We also observe a progressive reduction of the radar emission in correspondence of the shared frequencies, as well as an enhancement of the unlicensed jammer rejection capabilities. As a result, higher and higher SINR values can be achieved.

This is actually shown in Figure 3(c), where the normalized SINR is represented versus ϵ, assuming $E_I = 0.066$; namely, we consider, as figure of merit, SINR_n, which is defined as:

$$\text{SINR}_n = \frac{\text{SINR}}{|\alpha_T|^2} = \begin{cases} \boldsymbol{c}^{\star\,\dagger}\boldsymbol{R}\boldsymbol{c}^{\star}\,, & \text{for } \textbf{Algorithm 1} \\ \dfrac{|\tilde{\boldsymbol{g}}_0{}^{\dagger}\tilde{\boldsymbol{c}}_0|^2}{\tilde{\boldsymbol{g}}_0{}^{\dagger}\boldsymbol{M}\tilde{\boldsymbol{g}}_0}\,, & \text{for [10]} \end{cases} .$$

As expected, a proper choice of the design parameters will allow us to achieve good interference rejection properties as well as higher SINR values.

Notice that, starting from $\epsilon = 0.72$, with reference to our procedure, the maximum normalized SINR of the system is achieved. In fact,

$$\max_{\boldsymbol{c}} \boldsymbol{c}^{\dagger}\boldsymbol{M}^{-1}\boldsymbol{c} = \frac{1}{\lambda_{\min}(\boldsymbol{M})} \leq 1\,;$$

namely, SINR_n [dB] is upper-bounded by 0 dB.

In Figure 3(b), we provide a performance analysis in terms of autocorrelation properties of the designed waveforms. Evidently, better SINR values, spectral compatibility, and interference rejection are swapped for worse and worse range resolutions and/or ISLs/PSLs. It can be also observed that, as the auto-ambiguity properties of the transmit waveform of [10] are not directly under control, higher ISLs/PSLs values and, more in general, worse range-sidelobe profiles than the proposed approach can be experienced. Nevertheless, the smoother behavior of our signals agrees with our design criterion, since the optimization problem itself involves a compromise between the desire of lowering the transmitted energy in the stop-bands as well as in correspondence of the jammer central frequencies, and the need of keeping under control the ambiguity features of the sought signals.

In Figures 4, we analyze the ESD, the squared modulus of the ACF, and the normalized SINR of the waveforms devised for other three operative points (red dot, blue diamond, and green square of Figure 2). Specifically, we consider $(E_{I,n}, \hat{\epsilon})$, $n = 1, 2, 3$, with $E_{I,1} = 0.066$, $E_{I,2} = 0.216$, $E_{I,3} = 0.426$, and $\hat{\epsilon} = 0.264$. In Figure 4(a), we plot the ESD of the waveforms corresponding the three aforementioned points, together with the interference mask and the ESD of the reference code (notice that the curves for $E_{I,2}$ and $E_{I,3}$ actually overlap). As in the situation displayed in Figure 3(a), through **Algorithm 1**, the radar system has the ability to properly control the energy transmitted in the shared bandwidths, with a reduction of the ESD level, with respect to $\boldsymbol{c}_0$, up to 10 dB. Notice also that, when the allowed interference level E_I increases, more energy is transmitted in the stop-bands. However, since relaxing the energy constraint is tantamount to enlarging the feasible set, more degrees of freedom are available in this optimization process. They lead to smarter and smarter distributions of the useful energy at the unlicensed jammers frequencies: namely, we experience an enhancement in terms of unlicensed jammer rejection capabilities of the system which is a key ingredient to achieve better SINR values. This effect is shown in Figure 4(c), where the normalized SINR is plotted versus E_I, assuming $\epsilon = 0.264$. Evidently, as compared with the results reported in Figure 3(c), the maximum achieved normalized SINR is inferior.

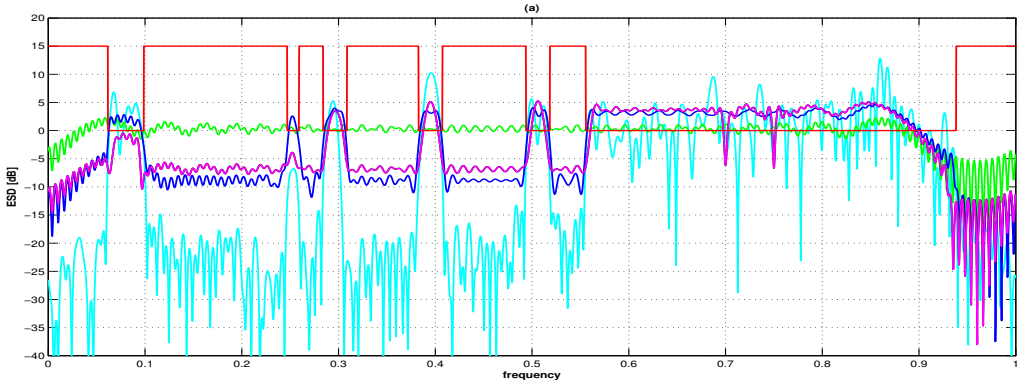

(a)

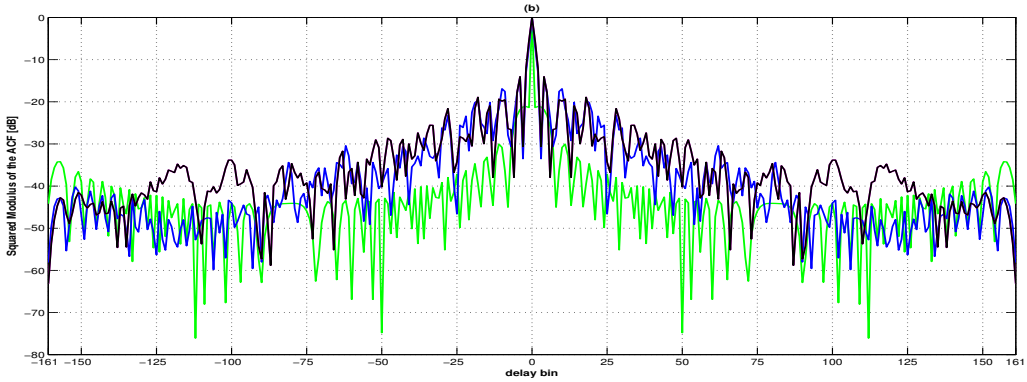

(b)

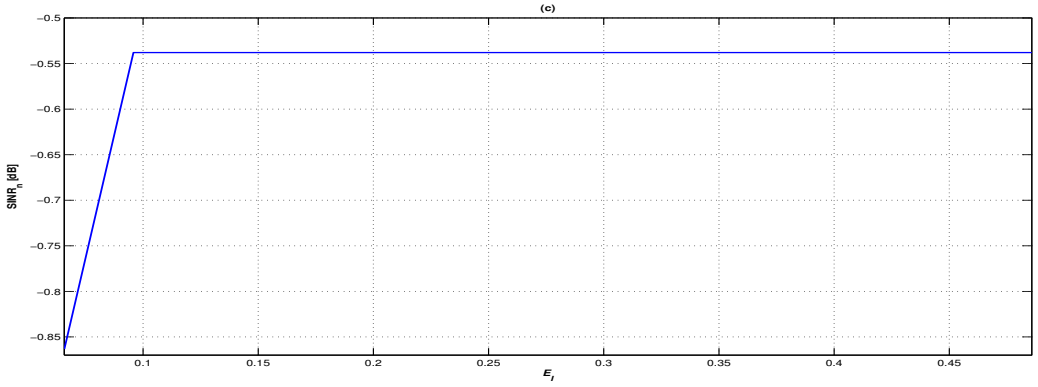

(c)

Figure 4: a) ESD; b) squared modulus of the ACF. red dash-dotted lines: stop-bands; green curve: reference code $\boldsymbol{c}_0$; blue curve: **Algorithm 1**, $E_I = 0.066$, $\epsilon = 0.264$; magenta curve: **Algorithm 1**, $E_I = 0.216$, $\epsilon = 0.264$; black curve: **Algorithm 1**, $E_I = 0.426$, $\epsilon = 0.264$ (notice that the magenta and the black curves partially overlap). c) Normalized SINR vs E_I, $\epsilon = 0.264$.

This can be justified observing that the disturbance suppression is less effective than that shown in Figure 3(a), due to the tighter similarity constraint.

Finally, in Figure 4(b) we report the squared moduli of the corresponding autocorrelations. Again, we can notice a trade-off, among the radar performance measures (namely, spectral coexistence capability, SINR, and ambiguity features), similar to that displayed in Figures 3.

References

[1] S. Blunt and H. Griffiths, "Spectrum Engineering and Waveform Diversity", *Tutorial at 2015 IEEE Radar Conference (RadarCon)*, Washington, DC, 11-15 May 2015.

[2] M. Wicks, "Spectrum Crowding and Cognitive Radar", *2010 2nd International Workshop on Cognitive Information Processing (CIP)*, pp. 452-457, Elba Island, Italy, 14-16 June 2010.

[3] L. S. Wang, J. P. McGeehan, C. Williams, and A. Doufexi, "Application of Cooperative Sensing in Radar - Communications Coexistence", *IET Proceedings on Radar, Sonar and Navigation*, Vol. 2, No. 6, pp. 856-868, July 2008.

[4] J. D. Taylor, *Ultra-Wideband Radar Technology*, CRC Press LLC, 2001.

[5] J. Salzman, D. Akamine, and R. Lefevre, "Optimal Waveforms and Processing for Sparse Frequency UWB Operation", *2001 IEEE Radar Conference (RadarCon)*, pp. 105-110, Atlanta, USA, 1-3 May 2001.

[6] C. Nunn and L. R. Moyer, "Spectrally-Compliant Waveforms for Wideband Radar", *IEEE Aerospace and Electronic Systems Magazine*, Vol. 27, No. 8, pp. 11-15, August 2012.

[7] K. Gerlach, "Thinned Spectrum Ultrawideband Waveforms Using Stepped-Frequency Polyphase Codes", *IEEE Transactions on Aerospace and Electronic Systems*, Vol. 34, No. 4, pp. 1356-1361, October 1998.

[8] I. W. Selesnick, S. U. Pillai and R. Zheng, "An Iterative Algorithm for the Construction of Notched Chirp Signals", *2010 IEEE Radar Conference (RadarCon)*, pp. 200-203, Washington DC, USA, 10-14 May 2010.

[9] I. W. Selesnick and S. U. Pillai, "Chirp-Like Transmit Waveforms with Multiple Frequency-Notches", *2011 IEEE Radar Conference (RadarCon)*, pp. 1106-1110, Kansas City, MO, USA, 23-27 May 2011.

[10] M. J. Lindenfeld, "Sparse Frequency Transmit and Receive Waveform Design", *IEEE Transactions on Aerospace and Electronic Systems*, Vol. 40, No. 3, pp. 851-861, July 2004.

[11] W. X. Liu, Y. L. Lu, and M. Lesturgie, "Optimal Sparse Waveform Design for HFSWR System", *2007 International Waveform Diversity and Design Conference*, pp. 127-130, Pisa, Italy, 4-8 June 2007.

[12] R. Kassab, M. Lesturgie, and J. Fiorina, "Alternate Projections Technique for Radar Waveform Design", *Radar Conference - Surveillance for a Safer World*, pp. 1-4, Bordeaux, France, 12-16 October 2009.

[13] H. He, P. Stoica, and J. Li, "Waveform Design with Stopband and Correlation Constraints for Cognitive Radar", *International Workshop on Cognitive Information Processing (CIP)*, pp. 344-349, Elba Island, Italy, 14-16 June 2010.

[14] G. Wang and Y. Lu, "Designing Single/Multiple Sparse Frequency Waveforms with Sidelobe Constraint", *IET Proceedings on Radar, Sonar and Navigation*, Vol. 5, No. 1, pp. 32-38, January 2011.

[15] L. Patton, C. A. Bryant, and B. Himed, "Radar-Centric Design of Waveforms with Disjoint Spectral Support", *2012 IEEE Radar Conference (RadarCon)*, pp. 1106-1110, Atlanta, GE, USA, USA, 269-274 May 2012.

[16] J. R. Guerci, *Cognitive Radar, The Knowledge-Aided Fully Adaptive Approach*, Artech House, 2010.

[17] S. Haykin, "Cognitive Radar: a Way of the Future", *IEEE Magazine on Signal Processing*, Vol. 23, No. 1, pp. 30-40, January 2006.

[18] S. Haykin, "Cognitive Dynamic Systems: Radar, Control, and Radio [Point of View]", *Proceedings of the IEEE*, Vol. 100, No. 7, pp. 2095-2103, July 2012.

[19] Y. Zhao, J. Gaeddert, K. K. Bae, and J. H. Reed, "Radio Environment Map-Enabled Situation-Aware Cognitive Radio Learning Algorithms", *Software Defined Radio (SDR) Technical Conference*, Orlando, FL, USA, November 2006.

[20] W. Ai, Y. Huang, and S. Zhang, "New Results on Hermitian Matrix Rank-One Decomposition", *Mathematical Programming*, Series A, Vol. 128, No. 1-2, pp. 253-283, June 2011.

[21] J. G. Proakis, M. Salehi, *Communication Systems Engineering*, Prentice-Hall Inc., 2002.

[22] Y. Zhao, J. H. Reed, M. Shiwen, K. K. Bae, "Overhead Analysis for Radio Environment Map-enabled Cognitive Radio Networks", *IEEE Workshop on Networking Technologies for Software Defined Radio Networks*, Reston, VA, USA, pp. 18-25, September 2006.

[23] T. Yucek and H. Arslan, "A Survey of Spectrum Sensing Algorithms for Cognitive Radio Applications", *IEEE Communications Surveys and Tutorials*, Vol. 11, No. 1, pp. 116-130, First Quarter 2009.

[24] J. Li, J. R. Guerci, and L. Xu, "Signal Waveform's Optimal-under-Restriction Design for Active Sensing", *IEEE Signal Processing Letters*, Vol. 13, No. 9, pp. 565-568, September 2006.

[25] S. Boyd and L. Vandenberghe, *Convex Optimization*, Cambridge University Press, 2003.

[26] A. d'Aspermont and S. Boyd, *Relaxations and Randomized Methods for Nonconvex QCQPs*, Stanford Univ., Stanford, CA, 2003, EE392o Class Notes.

[27] A. Ben-Tal and A. Nemirovski, *Lectures on Modern Convex Optimization: Analysis, Algorithms, and Engineering Applications*, MPS-SIAM Series on Optimization, 2001.

[28] H. Leong and B. Sawe, "Channel Availability for East Coast High Frequency Surface Wave Radar Systems", DREO TR 2001-104, Defence R&D Canada, Technical Report, November 2001.

[29] R. A. Horn and C. R. Johnson, *Matrix Analysis*, Cambridge University Press, 1985.

[30] A. Aubry, A. De Maio, A. Farina, and M. Wicks, "Knowledge-Aided (Potentially Cognitive) Transmit Signal and Receive Filter Design in Signal-Dependent Clutter", *IEEE Transactions on Aerospace and Electronic Systems*, Vol. 49, No. 1, pp. 93-117, January 2013.

[31] A. Aubry, A. De Maio, M. Piezzo, A. Farina, and M. Wicks, "Cognitive Design of the Receive Filter and Transmitted Phase Code in Reverberating Environment", *IET Radar, Sonar and Navigation*, Vol. 6, No. 9, pp. 822-833, December 2012.

[32] A. De Maio, Y. Huang, M. Piezzo, S. Zhang, and A. Farina, "Design of Optimized Radar Codes With a Peak to Average Power Ratio Constraint", *IEEE Transactions on Signal Processing*, Vol. 59, No. 6, pp. 2683-2697, June 2011.

[33] D. P. Bertsekas, *Nonlinear Programming, 2nd ed.*, Belmont, MA: Athena Scientific, 1999.

[34] J. Li, P. Stoica, and Z. Wang, "Doubly Constrained Robust Capon Beamformer", *IEEE Transactions on Signal Processing*, Vol. 52, No. 9, pp. 2407-2423, September 2004.

[35] A. Wenbao and S. Zhang, "Strong Duality for the CDT Subproblem: a Necessary and Sufficient Condition", *SIAM Journal on Optimization*, Vol. 19, No. 4, pp. 1735-1756, 2009.